0026-895X/07/7106-1512–1524$20.00
MOLECULAR PHARMACOLOGY
Copyright © 2007 The American Society for Pharmacology and Experimental Therapeutics
Mol Pharmacol 71:1512–1524, 2007

Vol. 71, No. 6
34645/3213164
Printed in U.S.A.

Mutation Studies of Ser7.39 and Ser2.60 in the Human CB_1 Cannabinoid Receptor: Evidence for a Serine-Induced Bend in CB_1 Transmembrane Helix 7

Ankur Kapur, Dow P. Hurst, Daniel Fleischer, Rob Whitnell, Ganesh A. Thakur, Alexandros Makriyannis, Patricia H. Reggio, and Mary E. Abood

California Pacific Medical Center Research Institute, San Francisco, California (A.K., D.F., M.E.A.); Center for Drug Design, Department of Chemistry and Biochemistry, University of North Carolina Greensboro, Greensboro, North Carolina (D.P.H., R.W., P.H.R.); Center for Drug Discovery, Northeastern University, Boston, Massachusetts (G.T., A.M.); and Department of Chemistry, Guilford College, Greensboro, North Carolina (R.W.)

Received January 30, 2007; accepted March 23, 2007

ABSTRACT

Ligands of structurally diverse natures are able to bind at the CB_1 cannabinoid receptor, suggesting the existence of multiple binding sites on the receptor. Modeling studies have implicated Ser2.60(173) and Ser7.39(383) as possible interaction site(s) for CB_1 agonists. To test the importance of these residues for receptor recognition, recombinant human CB_1 receptors, stably expressed in human embryonic kidney 293 cells, were used to investigate the consequences of mutating Ser2.60 (to S2.60A) or Ser7.39 (to S7.39A) in radioligand binding and guanosine 5′-3-*O*-(thio)triphosphate functional assays. The S7.39A mutant resulted in a total ablation of [^{3}H](−)-3-[2-hydroxyl-4-(1,1-dimethylheptyl)phenyl]-4-[3-hydroxylpropyl] cyclohexan-1-ol (CP55,940) high-affinity binding. However, [^{3}H](*R*)-(+)-[2,3-dihydro-5-methyl-3-[(4-morpholinyl)methyl]-pyrrolo[1,2,3-*de*]-1,4-benzoxazin-6-yl](1-naphthalenyl)methanone (WIN55,212-2) binding properties at S7.39A were comparable with those of the wild-type (WT) receptor. The binding affinity of (−)-11β-hydroxy-3-(1′,1′-dimethylheptyl)hexahydrocannabinol (AM4056) and (−)-11-hydroxydimethylheptyl-Δ^8-tetrahydrocannabinol (HU210) were drastically reduced (50- to 100-fold) at the S7.39A mutant. Likewise, the EC_{50} for HU210 and AM4056-mediated activation of the S7.39A receptor was increased by >200-fold. In contrast, the binding affinity and potency of WIN55,212-2, CP55,940, HU210, and AM4056 were unaltered at the S2.60A mutant compared with WT human CB_1 receptors. These results clearly suggest that Ser7.39, but not Ser2.60, plays a crucial role in mediating ligand specific interactions for CP55,940, HU210, and AM4056 at the human CB_1 receptor. Our modeling studies predict that Ser7.39 in a $g-\chi 1$ conformation may induce a helix bend in TMH7 that provides docking space for CP55,940 binding; the S7.39A mutation may alter this binding space, precluding CP55,940 binding.

The CB_1 cannabinoid receptor is a member of the G-protein coupled receptor (GPCR) family 1A, which includes the CB_2 receptor and the prototype rhodopsin (Howlett et al., 2002; Reggio, 2005). The human CB_1 and CB_2 receptors share only 44% amino acid overall homology, with a higher homology (68%) within the seven transmembrane domains (Munro et al., 1993). Both the CB_1 and CB_2 receptors share common signal transduction pathways, such as negative modulation of adenylyl cyclase activity (Felder et al., 1995) and also share certain common structural features with rhodopsin, including an extracellularly oriented N terminus, an intracellular carboxyl terminus, and hydrophobic transmembrane helices (TMHs).

Although neither CB_1 nor CB_2 proteins have been crystallized, the crystal structure of rhodopsin (Palczewski et al., 2000) serves as a valuable template to model the putative CB_1 ligand binding domains. Ligands of structural diverse

This study was supported by National Institutes of Health grants DA09978 and DA05274 (to M.E.A.), DA00489 and DA039434 (to P.H.R.), and DA09158 (to A.M. and M.E.A.).
Article, publication date, and citation information can be found at http://molpharm.aspetjournals.org.
doi:10.1124/mol.107.034645.

ABBREVIATIONS: GPCR, G-protein coupled receptor; TMH, transmembrane helix; CP55,940, (1*R*,3*R*,4*R*)-3-[2-hydroxy-4-(1,1-dimethylheptyl)-phenyl]-4-(3-hydroxypropyl)cyclohexan-1-ol; AAI, aminoalkylindole; WIN55,212-2, (*R*)-(+)-[2,3-dihydro-5-methyl-3-[(4-morpholinyl)methyl]pyrrolo[1,2,3-*de*]-1,4-benzoxazin-6-yl](1-naphthalenyl)methanone; SR141716A, *N*-(piperidin-1-yl)-5-(4-chlorophenyl)-1-(2,4-dichlorophenyl)-4-methyl-1*H*-pyrazole-3-carboxamide; HU-210, (−)-11-hydroxydimethylheptyl-Δ^8-tetrahydrocannabinol; AM841, (−)-7′-isothiocyanato-11-hydroxy-1′,1′-dimethylheptylhexahydrocannabinol; AM4056, (−)-11β-hydroxy-3-(1′,1′-dimethylheptyl)hexahydrocannabinol; GTPγS, guanosine 5′-3-*O*-(thio)triphosphate; (+)-7-OH-CBD-DMH, 7-OH-cannabidiol, 1,1-dimethylheptyl; CB, cannabinoid receptor; WT, wild type; HEK, human embryonic kidney; CM, conformational memories; Rho, rhodopsin; MD, molecular dynamics; EC, extracellular; IC, intracellular; h, human; SAH, southern aliphatic hydroxyl; NAH, northern aliphatic hydroxyl; HU-243, 3-dimethylheptyl-11-hydroxyhexahydrocannabinol.

classes recognize binding site(s) at the CB_1 receptors and confer a spectrum of efficacy ranging from agonism to antagonism and inverse agonism. These include: classic cannabinoid agonists [such as (−)-*trans*-δ-9-tetrahydrocannabinol], nonclassic cannabinoid agonists (such as CP55,940), endocannabinoids (such as *N*-arachidonoylethanolamine, anandamide), aminoalkylindole (AAI) agonists (such as WIN55,212-2), and diaryl pyrazole antagonist/inverse agonists (such as SR141716A) (Picone et al., 2002). Computational and mutational studies have identified several key amino acid residues in discrete noncontiguous regions of the TMHs that contribute in forming ligand binding sites (Abood, 2005; Reggio, 2005). These include but are not limited to the Lys3.28 (192), involved in the binding of anandamide, CP55,940, HU210, and SR141716A but not WIN55,212-2 (Song and Bonner, 1996; Chin et al., 1998; Hurst et al., 2002) via a hydrogen bonding interaction with the ligand. An aromatic microdomain contributed by Phe3.36, Trp4.64, Tyr5.39, Trp5.43, and Trp6.48 is involved in the binding of WIN55,212-2 and SR141716A (McAllister et al., 2002, 2003, 2004). Cys7.42 has been shown to be part of the binding pocket for SR141716A (Fay et al., 2005). Mutation of Leu3.43 of the human CB_1 (hCB_1) receptor was shown to increase the affinity of agonists and reduce the affinity of inverse agonist, suggesting that this residue plays a role in the coupling between the active and resting state of the receptor (D'Antona et al., 2006). Recent studies have suggested the existence of allosteric binding sites that modulate receptor function remotely by altering the affinity at orthosteric binding site(s) (Price et al., 2005). These studies indicate the existence of multiple ligand binding sites at the CB_1 receptor and warrant a detailed look at putative binding sites.

In this study, we have investigated the effects of mutation of two residues in TMH 2 and TMH 7, Ser2.60(173) and Ser7.39(383), respectively, on receptor structure and function. Ser2.60 and Ser7.39 are conserved in hCB_1 and hCB_2 receptors (Fig. 1A). Furthermore, both Ser2.60 and Ser7.39 are located at the top of their helixes toward the extracellular region, making them accessible to ligands (Fig. 1B). Modeling studies have predicted that AM841, an isothiocyanate derivatized classic ligand for the CB_1 receptor, establishes a hydrogen bonding interaction through its phenolic hydroxyl group with Lys3.28 (192), its 11-hydroxyl group with Ser2.60(173), and its pyran oxygen with Ser7.39(383) (Picone et al., 2005). Our results demonstrate that mutation of Ser7.39 has a significant effect on ligand affinity and potency of the nonclassic agonist CP55,940, the classic agonist HU210, and AM4056. In contrast, recognition of WIN55,212-2 and SR141716A are unaltered at the S7.39A receptor.

The loss of high-affinity CP55,940 binding at the S7.39(383)A mutant suggests the introduction of a steric block, one that cannot be caused by greater bulk of the mutated residue side chain because the Ser-to-Ala substitution is a size conservative change. Therefore, we hypothesized that Ser7.39(383) could produce a conformational effect on TMH7. The hydrogen-bonding capacity of Ser residues in α-helices can be satisfied by an intrahelical hydrogen bond interaction, in either the $g-$ or $g+$ conformation, between the O-γ atom and the *i*-3 or *i*-4 carbonyl oxygen (Gray and Matthews, 1984; Gratkowski et al., 2001). Ser residues in the $g-$ conformation can induce a bend in an α-helix (Ballesteros et al., 2000), and we have found that changes in wobble angle and face shift can also occur (Zhang et al., 2005). Our modeling studies suggest that Ser7.39(383) in a $g-$ $\chi 1$ conformation may induce a helix bend in TMH7 that provides space for the binding of CP55,940 and that mutation of Ser7.39(383) to Ala may alter this binding region space, precluding CP55,940 binding.

Materials and Methods

Materials

[^{3}H]WIN55,212-2 (40 Ci/mmol), [^{3}H]CP55,940 (160.6 Ci/mmol), and [^{35}S]GTPγS (1250 Ci/mmol) were purchased from PerkinElmer Life and Analytical Sciences (Boston, MA). WIN55,212-2, CP55,940, and SR141716A were obtained from Tocris (Ellisville, MO). HU-210 and (+)-7-OH-CBD-DMH was a generous gift from Dr. Raphael Mechoulam (Hebrew University, Jerusalem, Israel). AM4056 was synthesized by Dr. Alex Makriyannis (Northeastern University, Boston, MA). *Pfu* Turbo DNA polymerase for mutagenesis experiments was from Stratagene (La Jolla, CA). All other reagents were obtained from Sigma or other standard sources.

Amino Acid Numbering

The numbering scheme suggested by Ballesteros and Weinstein (1995) was employed here. In this system, the most highly conserved residue in each TMH is assigned a locant of 0.50. This number is preceded by the TMH number and followed in parentheses by the sequence number. All other residues in a TMH are numbered relative to this residue.

Mutagenesis and Cell Culture

The S2.60A and S7.39A mutants of the human CB_1 in the pcDNA3 vector were constructed using the QuikChange site-directed mutagenesis kit (Stratagene). Synthetic oligonucleotide mutagenic

	2.60									7.39		
hCB_1	V	Y	S	F	I	D	-	F	C	S	M	L
hCB_2	A	C	S	F	V	N	-	F	C	S	M	L
Rho	F	T	S	T	L	F	-	I	P	A	F	F

A

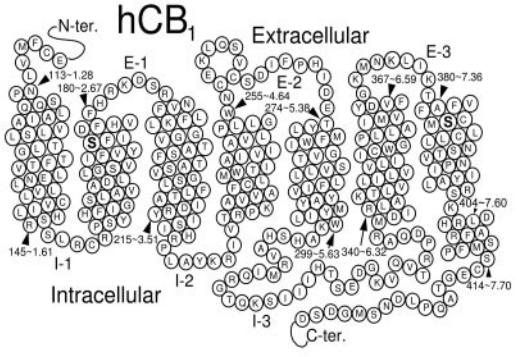

B

Fig. 1. A, amino acid sequence alignment of residues from hCB_1 and hCB_2 receptors and rhodopsin (Rho). Numbering shown is for hCB_1 receptor based on the scheme suggested by Ballesteros and Weinstein (1995) (*Materials and Methods*). B, schematic representation of the hCB_1 receptor structure and its seven transmembrane signaling regions. Also represented are the residues Ser2.60 and Ser7.39 (highlighted in bold), which lie at the top of transmembrane helices 2 and 7, respectively.

primers were typically 25 to 35 base pairs long (with 12–17 base pairs on either side of the desired mismatch region). Restriction endonuclease digestion and DNA sequencing were subsequently used to ascertain the presence of the mutation.

Stably transfected HEK-293 cell lines were created by transfection with wild-type or mutant CB_1-pcDNA3 cDNA with the use of the Lipofectamine reagent (Invitrogen, Carlsbad, CA) and selected in growth medium containing Geneticin (1 mg/ml) (Invitrogen) as described previously (Tao et al., 1999).

Radioligand Binding and GTPγS Binding Assay

Protein membrane preparations from harvested HEK293 cells were prepared and assayed as described previously (Tao et al., 1999; McAllister et al., 2004). In brief, binding assays (saturation binding and competition binding assays) were initiated by the addition of 50 μg of membrane protein to glass tubes pretreated with siliconizing fluid (to reduce nonspecific binding; Pierce, Rockford, IL) containing [^{3}H]WIN55,212-2 or [^{3}H]CP55,940 and an appropriate volume of binding buffer A (50 mM Tris-Base, 1 mM EDTA, 3 mM $MgCl_2$, and 5 mg/ml bovine serum albumin, pH 7.4) to bring the final volume to 500 μl. Nonspecific binding was determined in presence of excess (1 μM) nonradioactive WIN55,212-2 or CP55,940. Reactants were allowed to reach equilibrium. Subsequently, free and bound radioligands were separated by vacuum filtration through Whatman GF-C filters, and the radioactivity retained on the filters was determined by a liquid scintillation counter. Saturation binding experiments for [^{3}H]WIN55,212-2 or [^{3}H]CP55,940 at the hCB_1 receptor were conducted using concentrations ranging from 250 pM to 10 nM. In competition binding assays, the concentration of [^{3}H]WIN55,212-2 or [^{3}H]CP55,940 used paralleled their K_d value, determined earlier.

The K_d (equilibrium dissociation constant) and B_{max} (maximal binding) values were determined from saturation binding assays by nonlinear regression, and the data were fitted to one-site binding model using Prism 4.0 software (GraphPad, San Diego, CA). Displacement log IC_{50} values were determined by nonlinear regression and by fitting the data to one-site competition and then converted to K_i (inhibitory constant) value using the Cheng and Prusoff (1973) method and analyzed with the use of GraphPad Prism.

The GTPγS assay was initiated by the addition of 20 μg of membrane protein into silanized glass tubes containing 0.1 nM [^{35}S]GTPγS, 10 μM GDP in GTPγS binding buffer (50 mM Tris-HCl, 100 mM NaCl, 3 mM $MgCl_2$, 0.2 mM EGTA, and 0.1% bovine serum albumin, pH 7.4). Nonspecific binding was assessed in the presence of 20 μM unlabeled GTPγS. The reactants were equilibrated for 90 min at 30°C with various concentrations of ligands in a total volume of 500 μl to obtain a concentration-effect curve. Free and bound radioligands were separated by vacuum filtration through Whatman GF-C filters, and the radioactivity was determined by a liquid scintillation counter. Nonlinear regression of log concentration values versus percentage effect, fitted to sigmoidal dose-response, was used to obtain estimates of agonist concentrations that elicit half the maximal response (EC_{50}) and maximal response (E_{max}).

Statistical Analyses

Data are reported as mean value of the replicates along with their 95% confidence limits. The K_i and log EC_{50} values in the mutant and wild-type CB_1 receptors were compared using unpaired student's t test to determine the level of significance. P values of <0.05 were deemed to be statistically significant.

Molecular Modeling

Definition of Rotameric State of χ1. Different nomenclatures have been used to define the rotameric state of side-chain torsion angles. The nomenclature employed here for the χ1 torsion angle is that described by Shi et al. (2002). When the heavy atom at the γ position is at a position opposite the backbone nitrogen when viewed from the β-carbon to the α-carbon, the χ1 is defined to be *trans*. When the heavy atom at the γ position is at a position opposite the backbone carbon when viewed from the β-carbon to the α-carbon, the χ1 is defined to be *gauche*+ (*g*+). When the heavy atom at the γ position is at a position opposite the α-hydrogen when viewed from the β-carbon to the α-carbon, the χ1 is defined to be *gauche*− (*g*−). Using this nomenclature system, the side chain conformations discussed here are categorized into *g*− (0° < χ1 < 120°), *trans* (120° < χ1 < 240°), or *g*+ (240° < χ1 < 360°).

Conformational Memories (CM). *CM study of WT CB_1 TMH7.* We explored the possible conformational consequences in CB_1 TMH7 [Thr7.33(377)–Ser7.57(401)] of Ser7.39(383) at a *g*− χ1 by using the Monte Carlo/simulated annealing conformational memories (CM) method (Guarnieri and Weinstein, 1996). The conformational memories technique employs multiple Monte Carlo simulated annealing random walks using the CHARMM19 united atom force field. TMH7 from our published R* model of CB_1 (Picone et al., 2005) was used as a starting structure for the CM runs. All calculations were performed using a distance-dependent dielectric. 108 torsion angles of WT TMH7 were allowed to vary during the CM runs. These included the helix backbone φ and ψ and amino acid side chain torsion angles for residues Thr7.33–Ser7.57. The backbone φ and ψ in the region of Ser7.39(383) (Ala7.36–Cys7.42) were allowed to vary ± 50°. All other backbone torsion was allowed to vary ± 10°. Side-chain torsions were also allowed to vary ± 180° without constraints, except that the χ1 of Ser7.39(383) was set to *g*− and was not varied during the runs. The calculation was performed in two phases as indicated below.

Exploratory phase. In the exploratory phase, a random walk was used to identify the region of conformational space that is populated for each torsion angle studied. Starting at a temperature of 2070 K, 48,000 steps were applied to the rotatable bonds with cooling in 18 steps to a final temperature of 310 K. Trial conformations were generated at each temperature by randomly picking three torsion angles from the set of 108 and changing each angle by a random value within the range set in the calculation (see *CM study of WT CB_1 TMH7*). After each step, the generated trial conformation was either accepted or rejected using the Metropolis criterion. This calculation was repeated for a total of 128 cycles. Accepted conformations were used to map the conformational space of TMH7 by creating "memories" of values for each torsion angle that was accepted.

Biased Annealing Phase. In the second phase of the CM calculation, the only torsion angle moves attempted were those that would keep the angle in the "populated conformational space" mapped in the exploratory phase. The Biased Annealing phase began at a temperature of 721 K cooling to 310 K in 8 steps. One hundred twenty-eight structures were written out at 310 K.

S7.39(383)A mutant TMH7 CM runs. The conformational memories protocol used to explore the possible conformations of the S7.39(383)A mutant TMH7 was identical to that detailed above, except that all side-chain torsions were allowed to vary ± 180° without constraints.

Analysis of Output. Finally, the output of 128 WT TMH7 or S7.39(383)A TMH7 structures at 310 K was clustered using X-Cluster in MacroModel (Mohamadi et al., 1990). This program re-orders the structures according to their root-mean-square deviation and groups the structures into families of similar conformers.

The resulting 128 structures from CM were also analyzed using ProKink software (Visiers et al., 2000). This program, which is embedded in the Simulaid Conversion software (http://inka.mssm.edu/~mezei/simulaid/), was used to calculate the face shift, wobble, and bend angles of each helix.

Receptor Models. *Model of CB_1 WT inactive state (R) and activated state (R*) forms.* Our model of the inactive (R) form of CB_1 was created using the 2.8-Å crystal structure of bovine rhodopsin (Rho) (Palczewski et al., 2000). First, the sequence of the human CB_1 receptor (Gérard et al., 1991) was aligned with the sequence of bovine Rho using as alignment guides the same highly conserved residues that were used initially to generate our first model of CB_1 (Bramblett et al., 1995). TMH5 in CB_1 lacks the highly conserved

proline present in TMH5 of Rho (Leucine at position 5.50 in CB_1). The sequence of CB_1 in the TMH5 region was aligned with that of Rho as described previously using its hydrophobicity profile (Bramblett et al., 1995). Changes to the general Rho structure that were necessitated by sequence divergences included the absence of helix kinking proline residues in TMH1 and TMH5, the lack of a GG motif in TMH2 (at position 2.56 and 2.57), as well as the presence of extra flexibility in the TMH6 CWXP motif because of the presence of Gly6.49 immediately before Pro6.50 (Barnett-Norris et al., 2002). Further detail concerning this model is provided in our recent article (Hurst et al., 2006).

The crystal structure of rhodopsin represents the inactive state of the receptor (Palczewski et al., 2000; Okada et al., 2002; Li et al., 2004). The time scale for GPCR activation has been estimated to be milliseconds for light activation of rhodopsin (Arnis et al., 1994) but seconds for activation of the β2-adrenergic receptor by its diffusible ligand (Ghanouni et al., 2001) and in living cells (Nakanishi et al., 2006). It is not possible at the present time to perform molecular dynamics (MD) simulations to study agonist-induced changes to the inactive (R) state to generate the activated (R*) state because of the long timescales for GPCR activation compared with the typical length of MD simulations (10–100 ns). Although current research efforts are directed toward obtaining a structure of the rhodopsin activated state, (Meta II) (Schertler, 2005; Salom et al., 2006; Szundi et al., 2006), our present primary structural information about the GPCR activation process comes from biophysical studies of Rho and the β2-adrenergic receptor. For this reason, we have created a model of the CB_1 activated state (R*) based upon the documented changes that occur during the R-to-R* transition (Picone et al., 2005). The importance of the generation of such models has been discussed by Gouldson et al. (2004). These studies have indicated that rotation of both TMH3 and TMH6, as well as a conformational change in TMH6 (straightening in the CWXP hinge region of TMH6) occurs upon GPCR activation (Farrens et al., 1996; Lin and Sakmar, 1996; Javitch et al., 1997; Ghanouni et al., 2001; Jensen et al., 2001; Nakanishi et al., 2006). Recent in situ disulfide cross-linking studies (Ward et al., 2006) have confirmed an agonist-induced rotation of the cytoplasmic end of TMH6 in the M_3 muscarinic receptor.

An R* CB_1 model was therefore created by modification of our Rhodopsin-based model of the inactive (R) form of CB_1. This R* model construction was guided by the biophysical literature on the R-to-R* transition in rhodopsin (Rho), the β2-adrenergic and muscarinic M3 receptors, as discussed in the previous paragraph, and included a TMH6 conformer derived from our conformational memories study of CB_1 TMH6 (Barnett-Norris et al., 2002). Further detail concerning this model is provided in our recent article (Picone et al., 2005).

The CB_1 R* model was then refined by incorporation of a TMH7 conformation selected from the CM study reported here (bend angle = 15.1°, wobble = −164.6°, and faceshift = 9.0°). In addition, an R* model of the S7.39(383)A mutant was created by incorporation of a S7.39(383)A TMH7 conformation selected from the CM study reported here (bend angle = 8.2°, wobble = 57.0°, and faceshift = 15.4°) into the CB_1 R* model. Each conformer was superimposed at its intracellular end on the TMH7 included in our working model of the CB_1 R* state (for details of this model, see Picone et al., 2005). The original TMH7 was then deleted and the new TMH7 (either WT or S7.39(383)A mutant) was incorporated into the revised CB_1 R* model.

Ligand Docking Studies. Preliminary docking studies were performed in the TMH bundle before loop additions. Binding site conformations and anchoring interactions within the receptor used for each ligand were based on earlier published computational and experimental structure-activity relationship studies. HU210 and CP55,940 were docked in the global minimum energy conformation of their respective ring systems (Reggio et al., 1993; Tao et al., 1999) and, based on earlier data, Lys3.28(192) was used as the primary interaction site for the phenolic hydroxyl of each ligand. (Huffman et al., 1996; Song and Bonner, 1996). In the case of CP55,940, this interaction is supported by structure-activity relationship studies that showed a 40-fold loss of affinity upon removal of the phenolic -OH group of CP55,940 (Melvin et al., 1993). Such a profound affinity decrease suggests the loss of a strong hydrogen bond, such as one with a charged partner.

The energy of the ligand/CB_1 R* TMH bundle complex (or S7.39(383)A CB_1 R* TMH bundle) was minimized using the OPLS 2005 force field in Macromodel 9.1 (Schrödinger Inc., Portland, OR). An 8.0-Å extended nonbonded cutoff (updated every 10 steps), a 20.0-Å electrostatic cutoff, and a 40-Å hydrogen bond cutoff were used in each stage of the calculation. 6000 steps of conjugate gradient minimization in 500-step increments were employed with a distance-dependent dielectric. A 100 kcal/mol restraint was placed on all ϕ and ψ angles in TMH1–6 and Hx 8 and a 1000 kcal/mol harmonic restraint was placed on the TMH7 ϕ and ψ angles and on the TMH7 backbone bond angles. This protocol allowed the ligand and TMH bundle to draw together but preserved helix pitch and the conformational memories-calculated conformation of TMH7.

Modeling of Loops and N and C Termini. *Initial construction and refinement.* Extracellular (EC-1, His181–Ser185; EC-2, Cys257–Glu273; EC-3, Gly369–Lys376) and intracellular (IC-1, Ser146–Arg150; IC-2, Pro221–Val228; IC-3, Ala301–Pro332) loops, as well as portions of the N (Asn95–Asn112) and C termini (Ser414–Gly427), were then added to each refined model of the CB_1 WT R* and CB_1 S7.39(383)A R* bundles using the Loopy program within the protein structure modeling suite Jackal 1.5 (http://wiki.c2b2.columbia.edu/honiglab_public/index.php/Software:Jackal). The Modeler program was then used to refine loop structures (Sali and Blundell, 1993; Fiser et al., 2000).

EC-2 loop. One of the significant sequence divergences between Rho and CB_1 is in the second extracellular (EC-2) loop region. This loop in CB_1 is shorter than in Rho and is missing the conserved disulfide bridge between the cysteine in EC-2 and Cys3.25 in TMH 3 of Rho. Instead, there is a Cys residue at the extracellular end of TMH4 in CB_1 and a Cys near the middle of the E-2 loop that experiments suggest may form a disulfide bridge (Fay et al., 2005). Consequently, the position of the EC-2 loop with respect to the binding site crevice in CB_1 around TMHs 3-4-5 is likely to be quite different from that in Rho. For this reason, the refined EC-2 loop (Cys257–Glu273) structure built by Modeller was removed and the conformation of this loop was calculated using the biased scaled collective variable in Monte Carlo method (Hassan et al., 2002; Barnett-Norris et al., 2003). The aqueous environment of the EC-2 loop was modeled during these calculations with a recently developed implicit solvent model that is based on a screened Coulomb potential formulation (the screened Coulomb potential-implicit solvent model) during the loop conformational analysis (Hassan et al., 2000a,b). This loop was modeled with an internal Cys4.66(257)–Cys264 disulfide bridge based upon mutation results from the Farrens lab (Fay et al., 2005), which show that these two cysteines are required for high-level expression and receptor function.

IC-3 loop. The CB_1 IC-3 loop is much longer than the corresponding sequence in rhodopsin. NMR experiments have been performed on a peptide fragment composed of the CB_1 sequence span from the intracellular end of TMH5 to the intracellular end of TMH6, in micelles (Ulfers et al., 2002). This study suggested that part of the IC-3 loop is α helical. This region occurs after the intracellular end of TMH5 [Lys5.64(300)] and consists of a short α-helical segment from Ala301 to Arg307, followed by an elbow region (Arg307–Ile309) and an α-helical segment (Gln310–Ser316) up to an III (Ile317–Ile319) in IC-3. Based on these results, we replaced the initial Modeller-built IC-3 loop with this α-helix-elbow-α-helix region and then the rest of IC-3 loop (Ile317–Pro332) was rebuilt and optimized using Modeller.

Final energy minimization. The energy of the ligand/CB_1 R* complex, including loop regions and N and C termini, [or S7.39(383)A CB1 R* complex] was minimized using the OPLS 2005 force field in Macromodel 9.1 (Schrödinger Inc.). An 8.0-Å extended nonbonded

cutoff (updated every 10 steps), a 20.0-Å electrostatic cutoff, and a 4.0-Å hydrogen bond cutoff were used in each stage of the calculation. The minimization was performed in two steps. The first step consisted of 4000 steps of conjugate gradient minimization in 500-step increments using a distance-dependent dielectric. In this stage of the calculation, the helix bundle and ligand were allowed to optimize. No harmonic restraints were placed on the ligand so that it was free to move, and the transmembrane helices were free to move to optimize the ligand/receptor interaction. To preserve the pitch of the transmembrane helices, a 100 kcal/mol restraint was placed on all ϕ and ψ angles in TMHs 1–6 and Hx 8. To preserve the CM-calculated conformation of TMH7, a 1000 kcal/mol harmonic restraint was placed on the ϕ and ψ angles and on the TMH7 backbone bond angles. To preserve the loop conformations, a 1000 kcal/mol harmonic restraint was also placed on all loop atoms.

In the second stage of the calculation, the generalized born/surface area continuum solvation model for water as implemented in Macromodel was used. This stage of the calculation consisted of 4000 steps of Polak-Ribier conjugate gradient minimization in 500-step increments in which the ligand and transmembrane bundle were frozen, but the loops were allowed to relax.

Assessment of pairwise interaction energies. After defining the atoms of each ligand as one group (group 1) and the atoms corresponding to a residue that lines the binding site in the final ligand/CB_1 R* complex as another group (group 2), Macromodel (version 8.6) was used to output the pair-wise interaction energy (coulombic and van der Waals) for a given pair of atoms. The pairs corresponding to group 1 (ligand) and group 2 (residue of interest) were then summed to yield the interaction energy between the ligand and that residue.

Energy expense assessments for docked ligands. To calculate the energy difference between the global minimum energy conformer of each compound (i.e., the docked structure) and its final conformation after energy minimization of the ligand/receptor complex (the latter as listed in Tables 4 and 5), rotatable bonds in the global minimum energy conformation were driven to their corresponding value in the final docked conformation and the single point energy of the resultant structure was calculated at the HF 3–21G* level using Jaguar (version 6.0; Schrödinger).

Results

Radioligand Binding and Functional Assays

Saturation Binding Assays. The binding of [^{3}H]CP55,940 or [^{3}H]WIN55,212-2 to wild-type and mutant hCB_1 receptors, stably expressed in HEK-293 cells, was measured to generate an estimate of the equilibrium dissociation constant (K_d) and the maximal binding (B_{max}) values. Cell surface receptor expression of wild-type or mutant cell line was verified by immunocytochemistry with a polyclonal antibody to the N-terminal (1–14) of the hCB_1 receptor (data not shown). Cell lines that displayed levels of cell surface labeling comparable to that of the wild-type hCB_1 receptor were chosen for further analysis. CP55,940 was employed as one of the reporter radioligands for binding studies because its binding sites have been suggested to involve hydrogen bonding interactions with Lys3.28 through its southern aliphatic hydroxyl (SAH) group, the northern aliphatic hydroxyl (NAH) of CP55,940 with Lys2.60, and the phenolic hydroxyl of CP55,940 with Asp6.58 (McAllister et al., 2003; Salo et al., 2004)(Scheme 1). WIN55,212-2 (Scheme 1) was also employed as one of the radioligands as no binding was observed with CP55,940 at the S7.39A mutant receptor (see below). Furthermore, WIN55,212-2 binding sites at the CB_1 receptor are predicted not to involve the residues being investigated here because we have demonstrated previously that the binding pocket of WIN55,212-2 involves aromatic residues from the TMH 3-4-5-6 region (McAllister et al., 2003).

Saturation (equilibrium) binding analysis for [^{3}H]CP55,940 at the S2.60A mutant receptor generated K_d and B_{max} values of 4.2 nM and ~3 pmol/mg, respectively, that were not significantly different from that of the WT hCB_1 receptor (K_d, 2 nM; B_{max}, 1 pmol/mg) (Table 1). Likewise, K_d and B_{max} values of the radioligand [^{3}H]WIN55,212-2 on the Ser2.60A mutant were similar to those of the WT hCB_1 receptor (data

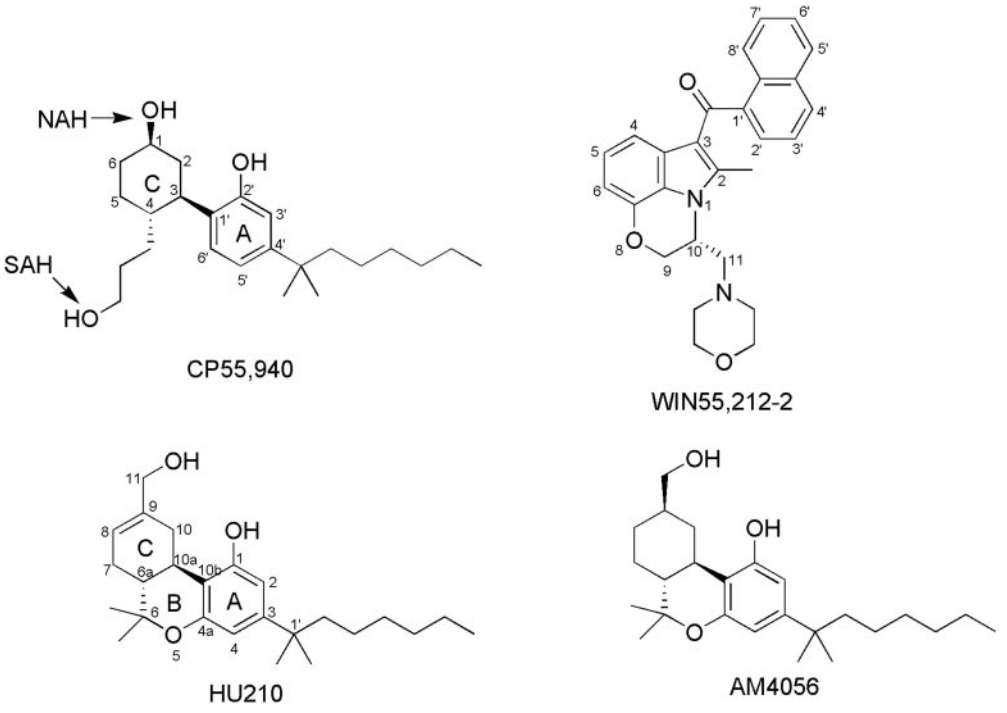

Scheme 1. Compounds evaluated in this study.

not shown). In contrast, the S7.39A mutant hCB_1 receptor resulted in total ablation of [^{3}H]CP55,940 binding. However, the K_d and B_{max} values of [^{3}H]WIN55,212-2 on the Ser7.39A mutant (6 nM and 1.9 pmol/mg, respectively) were comparable with the WT receptor (4.7 nM and 1.2 pmol/mg, respectively) (Table 1). Therefore, competition binding assays on the S7.39A mutant were performed using several structurally diverse cannabinoid ligands versus [^{3}H]WIN55,212-2 (see below).

Competition Binding Assays. The binding affinity of a series of structurally diverse cannabinoid ligands for wild-type and mutant hCB_1 were examined. The ability of AAI agonists (typified by WIN55,212-2), the nonclassic cannabinoid agonists (typified by CP55,940), the classic cannabinoid agonists [AM4056 (an analog of AM841) and HU210 (a dimethylheptyl analog of (−)-*trans*-δ-8-tetrahydrocannabinol)], and the biarylpyrazole inverse agonist/antagonist SR141716A to displace the reporter ligand [^{3}H]CP55,940 or [^{3}H]WIN55,212-2 bound to the wild-type or mutant hCB_1 receptor was used to calculate the inhibitory constant (K_i) value as described under *Materials and Methods*.

Figure 2 and Table 2 summarize the displacement of [^{3}H]WIN55,212-2 by WIN55,212-2, CP55,940, SR141716A, HU210, and AM4056 from WT and S7.39A mutant hCB_1. The K_i values of the agonist, WIN55,212-2 (Fig. 2A) and the inverse agonist, SR141716A (Fig. 2B) on the S7.39A mutant were comparable and not statistically different from the WT receptor. In contrast, a drastic, ~50- to 100-fold reduction in binding affinities of AM4056 (Fig. 2C) and HU210 (Fig. 2E) (K_i, ~21 and 46 nM, respectively) were observed at the S7.39A mutant receptor compared with the WT hCB_1 receptor (K_i, 0.37 and 0.45 nM, respectively). CP55,940 was unable to fully displace the reporter radioligand [^{3}H]WIN55,212-2 from S7.39A mutant; 40% displacement was observed at the highest concentration of the competing ligand CP55,940 (10 μM) (Fig. 2D). The displacement of [^{3}H]CP55,940 by WIN55,212-2, CP55,940, SR141716A, HU210, and AM4056 from WT and S2.60A mutant hCB_1 are summarized in Fig. 3, A to E, and Table 2. The K_i values of the ligands tested at the S2.60A mutant were similar to and not significantly different from the WT hCB_1 receptor, suggesting that residue Ser2.60 is not crucial in ligand recognition.

Functional Effects of Ser7.39 and Ser2.60 Mutations. The ability of ligands to stimulate the binding of [^{35}S]GTPγS was used as a marker to measure the activation of wild-type and mutant hCB_1 receptor (see Fig. 4, A–D). The WT hCB_1 receptor has EC_{50} values for WIN55,212-2, CP55,940, AM4056, and HU210-induced activation of ~5, 0.75, 0.03, and 0.07 nM, respectively (Table 3). The substitution of

TABLE 1

Radioligand binding properties of wild-type and mutant cell lines.

The K_d and B_{max} values were determined from saturation binding experiments using [^{3}H]CP55,940 or [^{3}H]WIN55,212-2 on HEK 293 cell membrane preparations stably transfected with wild-type or mutant hCB_1 receptor. Data represent the mean and corresponding 95% confidence limits of at least three independent experiments performed in triplicate. No significant difference was observed between the wild-type and mutant binding properties as determined by two-tailed Student *t* test.

Radioligand & Cell Line	K_d	B_{max}
	nM	*pmol/mg*
[^{3}H]CP55,940		
WT	2.0 (0.7–3.2)	1.03 (0.8–1.3)
S7.39A	N.B.	
S2.60A	4.2 (1.5–6.8)	3.3 (2.3–4.5)
[^{3}H]WIN55,212-2		
WT	4.7 (1.8–7.5)	1.2 (1.0–1.6)
S7.39A	6.0 (5.4–6.5)	1.9 (0.5–2.4)

N.B., no specific binding observed.

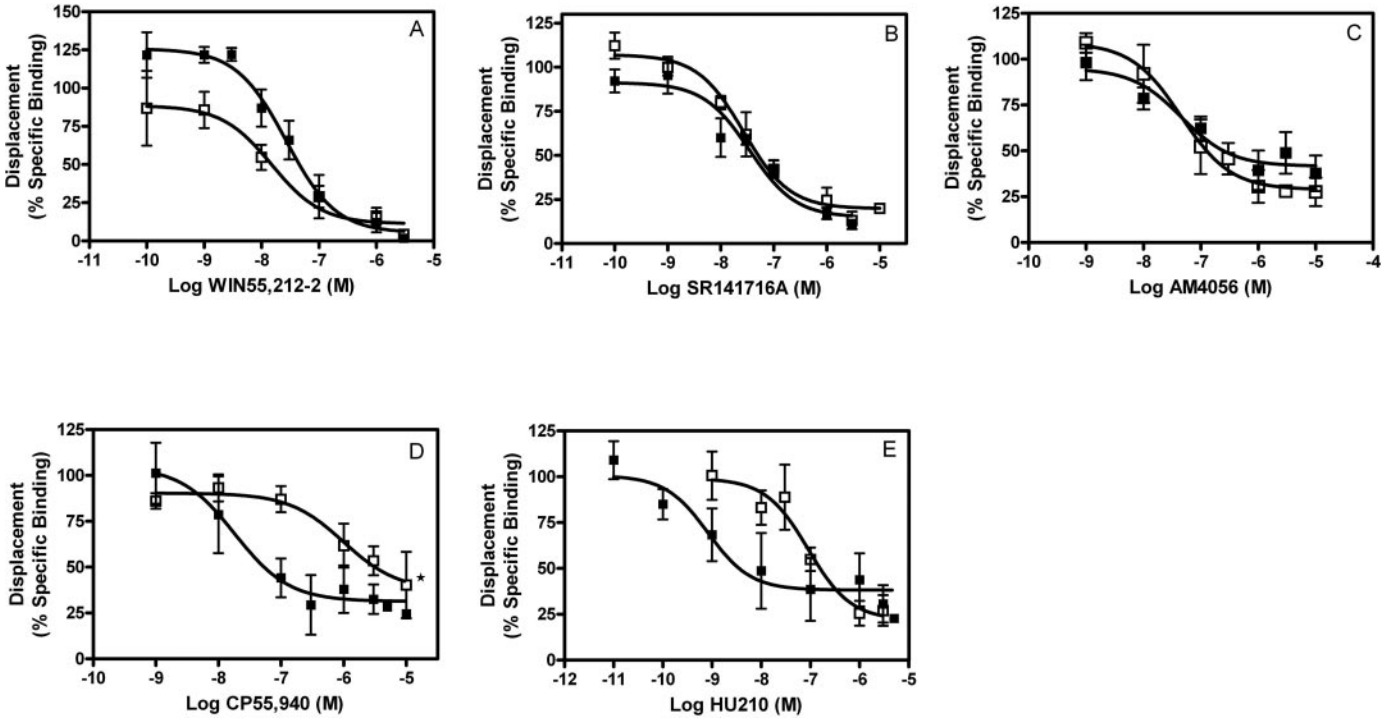

Fig. 2. Competitive displacement of [^{3}H]WIN55,212-2. WIN55,212-2 (A), SR141716A (B), AM4056 (C), CP55,940 (D), and HU210 (E) were used for displacing bound [^{3}H]WIN55,212-2 in membranes prepared from HEK 293 cells stably transfected with wild-type (■) or S7.39A mutant (□) CB_1 receptors. Each data point represents mean ± S.E.M. of at least three independent experiments performed in triplicate. It should be noted that CP55,940 at concentrations as high as 10 μM, was able to displace ~40% of bound [^{3}H]WIN55,212-2 (D) in the S7.39A mutant (*).

Ser2.60 with an alanine (S2.60A) did not significantly affect the concentration dependence of the agonist being investigated. Although modest reductions (~5-fold) in the potency of WIN55,212-2, CP55,940, and HU210 were observed, this was not statistically different from the WT hCB_1 receptor. However, significant rightward shifts in the concentration-effect curve were observed with the S7.39A mutant receptor for AM4056 and HU210. The EC_{50} values for AM4056- and HU210-mediated receptor activation increased to 16 nM (580-fold increase) and 14 nM (200-fold increase), respectively, representing a drastic reduction in agonist sensitivity. These changes in potency paralleled the reduced binding affinity observed (see Table 2). CP55,940 did not produce detectable GTPγS stimulation in the S7.39A mutant. In contrast, the EC_{50} value of WIN55,212-2-induced activation of the S7.39A mutant was unaltered and comparable with the WT hCB_1 receptor.

The intrinsic basal (constitutive) activities of the WT and the mutant hCB_1 receptors (S2.60A and S7.39A) were comparable (data not shown), suggesting that the mutation had not altered the resting to active state equilibrium of the receptors.

Modeling Studies

Conformational Memories Results: TMH7 Conformation in WT CB_1 and the S7.39(383)A Mutant. Figure 5 illustrates the results obtained from CM studies of WT CB_1 TMH7 (green) and the CB_1 S7.39(383)A mutant TMH7 (magenta). This figure depicts all 128 structures from both of the runs superimposed at their intracellular ends on TMH7 in our previous CB_1 R* model (Picone et al., 2005). When Ser7.39(383) (which is located on the interior face of TMH7) adopts a $g-\ \chi 1$, it causes the top portion of the helix to bend away from Ser7.39(383) (Fig. 5, inset). The net result is that the extracellular end of TMH7 pulls away from the TMH bundle. Replacement of Ser7.39(383) with an Ala results in the moderation of this kink (because of the lack of hydrogen-bonding capability of the Ala side chain), bringing the extracellular end of TMH7 more into the TMH bundle.

From these CM results, a new TMH7 for the WT bundle

TABLE 2

The effects of amino acid mutations of recombinant CB_1 receptors on the displacement of [^{3}H]WIN55,212-2 or [^{3}H]CP55,940 by cannabinoid receptor ligands

Data represent the mean and corresponding 95% confidence limits of at least three independent experiments performed in triplicate. Values reported are nanomolar except where indicated. Competition experiments for the S7.39A mutant were carried out against [^{3}H]WIN55,212-2, because no binding was observed with [^{3}H]CP55,940 on this mutant. On the S2.60A mutant, competition binding were performed against [^{3}H]CP55,940. Statistical analysis was performed by comparing the K_i of the mutant receptor to that of the wild-type CB_1 receptors (*, $P < 0.05$) using the Student t test to determine the level of significance.

	WIN55,212-2	SR141716A	CP55,940	HU210	AM4056
[^{3}H]WIN55,212-2					
WT	13.9 (7.2–27)	18.4 (8.2–41)	10.0 (1.3–74)	0.45 (0.07–3)	0.37 (0.12–1)
S7.39A	7.7 (2–28)	14.2 (7.8–25)	—[a]	45.7* (12–180)	20.6* (5.6–76)
[^{3}H]CP55,940					
WT	15.9 (9–28)	7.2 (3.2–16)	1.4 (0.8–2.4)	0.38 (0.25–0.58)	0.63 pM (0.1–3.6)
S2.60A	17.1 (5–59)	22.8 (13–40)	1.2 (0.2–8)	0.66 (0.13–0.34)	0.5 pM (0.04–5)

[a] At 10 μM CP55,940, 40% displacement was observed.

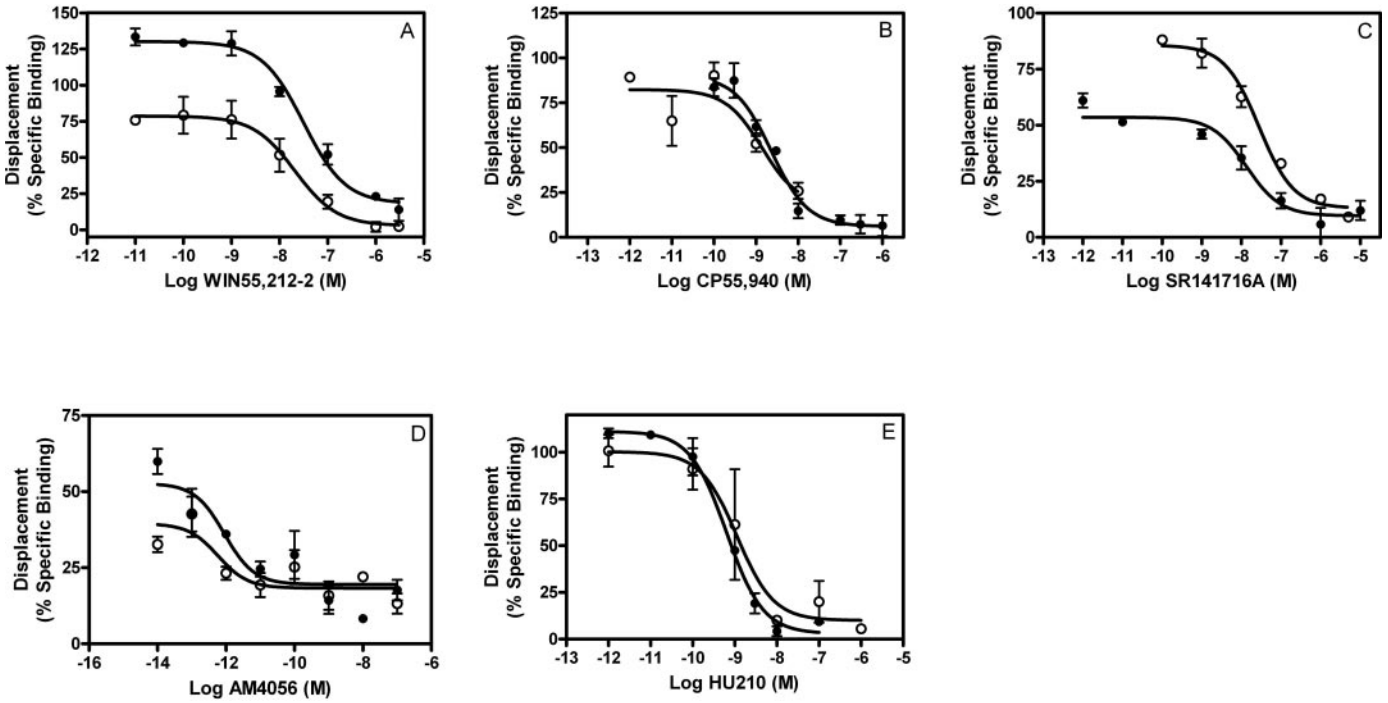

Fig. 3. Competitive displacement of [^{3}H]CP55,940. WIN55,212-2 (A), CP55,940 (B), SR141716A (C), AM4056 (D), and HU210 (E) were used for displacing bound [^{3}H]CP55,940 in membranes prepared from HEK 293 cells stably transfected with wild-type (●) or S2.60A mutant (○) CB_1 receptors. Each data point represents mean ± S.E.M. of at least three independent experiments performed in triplicate.

(bend angle = 15.1°, wobble = −164.6°, and faceshift = 9.0°) and a TMH7 for the S7.39(383)A mutant R* model (bend angle = 8.2°, wobble = 57.0°, and faceshift = 15.4°) was chosen. The conformations of these helices are consistent with the hypothesis that the presence of a Ser at position 7.39 in WT CB_1 TMH7 can induce a greater bend in WT CB_1 (15.1°) than possible in the S7.39(383)A mutant TMH7 (8.2°).

Receptor Docking Studies. Lys3.28(192) was used as the primary interaction site in CB_1 docking studies of HU210 and CP55,940 reported here based upon the K3.28(192)A mutation results of Song and Bonner (1996) and supported by subsequent studies (Chin et al., 1998). These studies showed a complete loss of HU210 and CP55,940 (but not WIN 55,212-2) binding and a >100-fold increase in EC_{50} value for receptor activation upon this mutation. Our modeling studies suggest that despite the fact that these two ligands use the same primary interaction site, the positions of these ligands within the CB_1 R* bundles are quite different. Figure 6 shows a comparison of the binding sites of HU210 and CP55,940 in the WT CB_1 R* model. Fig. 6, a and c, illustrate vertical views of the HU210 versus CP55,940 binding sites, respectively. The viewpoint in these figures is from TMHs 4 and 5 toward the ligand, with the extracellular loops shown at the top of each figure. TMHs 4 and 5 have been omitted from the figure for clarity. It is clear here that HU210 lies lower in the TMH bundle binding site crevice than does CP55,940.

HU210/CB_1 R* Complex. HU210 was docked in the global minimum energy conformation for its fused ring structure (Reggio et al., 1993), using Lys3.28(192) as its primary interaction site (Song and Bonner, 1996). In the energy-minimized HU210/CB_1 R* complex (Fig. 6, a and b), Lys3.28(192) acts as a hydrogen bond donor to the phenolic oxygen of HU210. The hydrogen bond (N-O) distance and (N-H--O) angle for this interaction are 2.69 Å and 164°. The northern aliphatic hydroxyl of HU210 hydrogen bonds with both Ser7.39(383) and Ser1.39(123). For the Ser7.39(383) hydrogen bond, the NAH hydroxyl group acts as the hydrogen bond donor to the serine oxygen. The hydrogen bond (O-O) distance and (O-H--O) angle are 2.65 Å and 175°. For the Ser1.39(123) hydrogen bond, the NAH hydroxyl oxygen acts as the hydrogen bond acceptor. The hydrogen bond (O-O) distance and (O-H--O) angle are 2.62 Å and 178°. As revealed in Table 4, the ligand has its greatest pairwise interaction energy with Ser7.39(383) (−7.19 kcal/mol), followed by Ser1.39(123) (−5.21 kcal/mol) and Lys3.28(192) (−4.70 kcal/mol). For these interactions, the coulombic energy dominates the overall pair-wise energy of interaction. The ligand also has significant interactions with Cys7.42(386) (−4.24 kcal/mol), Leu7.43(387) (−4.11 kcal/mol), and Phe2.57(170) (−4.09 kcal/mol). For the Cys7.42(386) and Leu7.43(387) interactions, the van der Waals energy dominates the overall energy of interaction. The Phe2.57(170) interaction has significant van der Waals and coulombic contributions and seems to have arisen from the interaction of phenolic ring hydrogens with the aromatic ring of Phe2.57(170). The energy difference between the initially docked HU210 conformation and the final conformation in the energy-minimized complex was found to be 0.59 kcal/mol at the HF 3–21G* level.

CP55,940/CB_1 R* Complex. CP55,940 was docked in the CB_1 R* model in its global minimum energy conformation. In the CP55,940/CB_1 R* complex (Fig. 6, c and d), the phenolic hydroxyl of CP55,940 hydrogen bonds with K3.28(192). The hydrogen bond (N-O) distance and (N-H--O) angle for this interaction are 2.67 Å and 154°. The NAH (Scheme 1) hydrogen bonds to Ser1.39(123). The hydrogen bond (O-O) distance and (O-H--O) angle for this interaction are 2.67 Å and 170°.

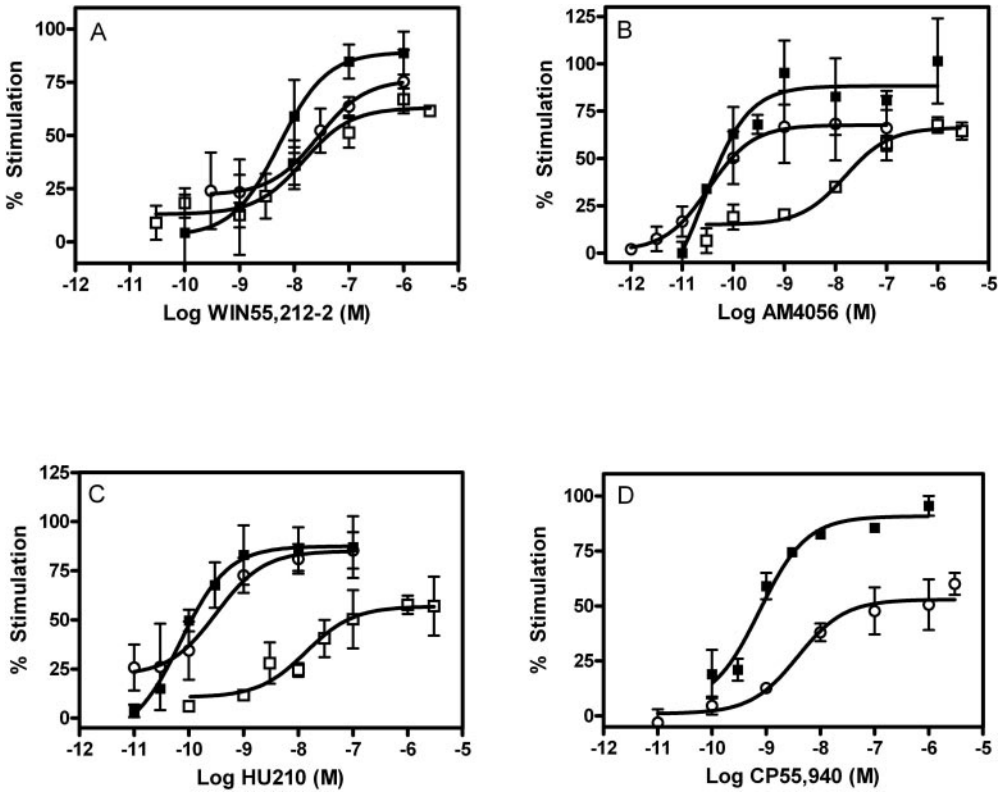

Fig. 4. Activation of wild-type and mutant receptors. WIN55,212-2 (A), AM4056 (B), HU210 (C) and CP55,940 (D). Concentration-effect curves obtained from [^{35}S]GTPγS binding in HEK membrane preparations expressing wild-type (■) or S7.39A (□) S2.60A mutant (○) CB_1 receptors. Each data point represents mean ± S.E.M. of at least three independent experiments performed in triplicate.

The SAH (Scheme 1) of CP55,940 forms two hydrogen bonds with Lys373 in the EC-3 loop. In the first hydrogen bond, Lys373 acts as the hydrogen bond donor to the SAH hydroxyl oxygen. The hydrogen bond (N-O) distance and (N-H--O) angle for this interaction are 2.93 Å and 165°. In the second hydrogen bond, the SAH hydroxyl hydrogen donates a hydrogen bond to the backbone carbonyl oxygen of Lys373. The hydrogen bond (O-O) distance and (O-H-O) angle are 2.92 Å and 166°. In this docked position, the carbocyclic A ring of CP55,940 (Scheme 1) is close to TMH7 at the level of Ser7.39(383). The pair-wise interaction energy summary in Table 5 shows that the ligand has its greatest pair-wise interaction energy with Lys373 (−14.91 kcal/mol), followed by Lys3.28(192) (−6.77 kcal/mol) and Ser1.39(123) (−5.67 kcal/mol). For these interactions, the coulombic energy dominates the overall energy of interaction. The ligand also has a significant interaction with Ser7.39(383) (−4.17 kcal/mol). This interaction has significant van der Waals and coulombic contributions and seems to have arisen from the interaction of phenolic ring hydrogens with the available serine side chain oxygen lone pairs of electrons [Ser7.39(383) in $g-\chi 1$]. The energy difference between the initially docked CP55,940 conformation and the final conformation in the energy-minimized complex was found to be 3.26 kcal/mol at the HF 3–21G* level.

TABLE 3

Concentration-effect data for agonist stimulation of [^{35}S]GTPγS of wild-type and mutant receptors expressed in HEK 293 cells

Data represent the mean of at least three independent experiments performed in triplicate. EC_{50} values were determined from concentration-effect curves using Prism software. The values in parentheses are the 95% confidence intervals (CI). Statistical analysis was performed by comparing the log EC_{50} of the mutant receptor with that of the wild-type CB_1 receptors using the Student t test to determine the level of significance.

Agonist & Cell Line	EC_{50} (CI)	Mutant/WT EC_{50}
WIN55,212-2		
WT	5.5 nM (1–30)	1
S7.39A	14.7 nM (4–53)	2.6
S2.60A	27 nM (5–140)	4.8
CP55,940		
WT	0.75 nM (0.3–1.7)	1
S7.39A	N.D.	
S2.60A	3.8 nM (1–15)	5
HU210		
WT	70.2 pM (22.4–220)	1
S7.39A	13.9 nM (2.5–76)*	198
S2.60A	317 pM (42–2300)	4.5
AM4056		
WT	26.8 pM (4–170)	1
S7.39A	15.6 nM (6.7–36)**	580
S2.60A	33.4 pM (3.3–300)	1.2

N.D., not detected
* $P < 0.05$;
** $P < 0.005$.

HU210/CB_1 S7.39(383)A R* Complex Modeling studies suggest that in addition to HU210's loss of a hydrogen-bonding interaction with Ser7.39(383) upon mutation to Ala, HU210 also loses its ability to hydrogen-bond with Ser1.39(123). This is due to the concomitant change in the shape of the TMH1-2-7 binding pocket, caused by the alteration in TMH7 conformation produced by the mutation (Fig. 7 and Table 4). It is clear in Fig. 7 that, because of the conformational shift in the extracellular end of TMH7, the extracellular ends of TMHs 1 and 2 are displaced as well to

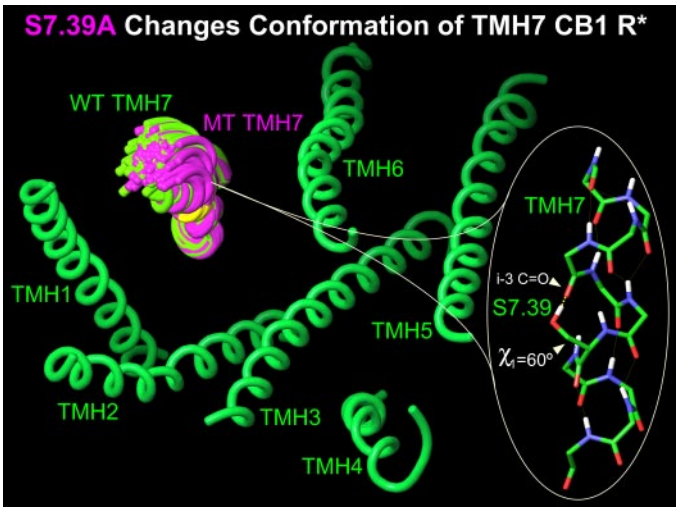

Fig. 5. Results obtained from CM studies of WT CB_1 TMH7 (green) and the CB_1 S7.39(383)A mutant TMH7 (magenta). All 128 structures from both of the CM runs are superimposed here at their intracellular ends on TMH7 in our previous CB_1 R* model, which is also shown in green (Picone et al., 2005). When Ser7.39(383) (which is located on the interior face of TMH7) adopts a $g-\chi 1$, it causes the top portion of the helix to bend away from Ser7.39(383) (inset). The net result is that the extracellular end of TMH7 pulls away from the TMH bundle. Replacement of Ser7.39(383) with an Ala results in the moderation of this kink (magenta helices) as a result of the lack of hydrogen bonding capability of the Ala side chain. This brings the extracellular end of TMH7 more into the TMH bundle.

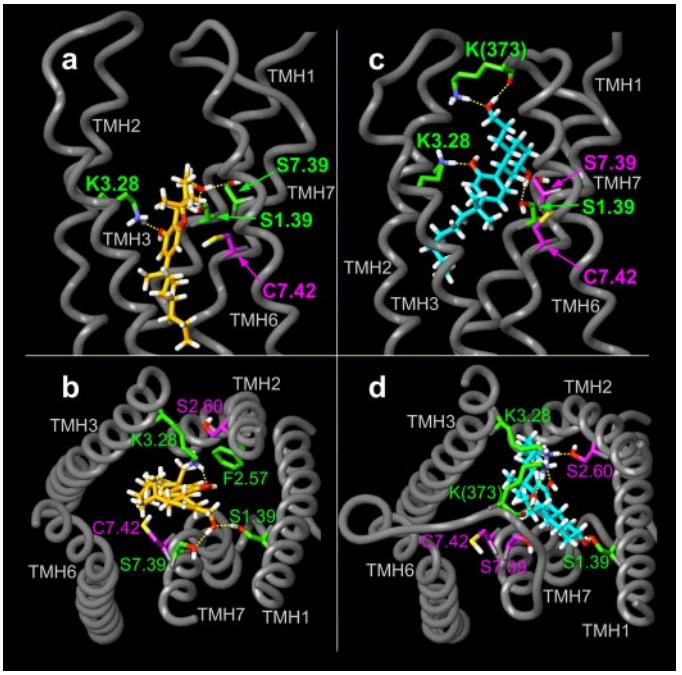

Fig. 6. A comparison of the binding sites of HU210 and CP55,940 in the WT CB_1 R* model. Residues that have significant coulombic interactions with each ligand are shown in green. Yellow dashed lines indicate hydrogen bonding interactions. Other selected residues are shown in magenta. a and c illustrate a vertical view of the HU210 versus CP55,940 binding sites, respectively. The viewpoint in these figures is from TMHs 4 and 5 toward the ligand, with the extracellular loops shown at the top of each figure. TMHs 4 and 5 have been omitted from the figure to simplify the view. Our modeling results suggest that whereas CP55,940 and HU210 bind in the TMH1-2-3-7 region of the CB1 WT binding pocket, CP55,940 binds higher (more extracellular) in this pocket (compare a and c). In this docked position, the carbocyclic A ring of CP55,940 (Scheme 1) is close to TMH7 at the level of Ser7.39(383) and is therefore poised to be affected by the inward movement of the extracellular end of TMH7 upon the S7.39(383)A mutation. b and d are views from the extracellular side of the receptor. Extracellular loops have been omitted here to simplify the view.

accommodate this change in TMH7. Here, the position of the helices in the Ser7.39(383) mutant are shown in cyan, whereas their positions in WT CB1 are shown in gray. The distance between the Ser1.39(123) hydroxyl oxygen and the HU210 NAH hydroxyl oxygen is 4.99 Å, thus precluding the formation of a hydrogen bond in the S7.39(383)A mutant. No significant shift was seen for any other TMH in the S7.39(383)A mutant TMH bundle relative to the WT TMH bundle.

Only one hydrogen bond [to Lys3.28(192)] remains for HU210 in the S7.39(383)A mutant. Here, Lys3.28(192) acts as a hydrogen bond donor to the phenolic hydroxyl oxygen of HU210. The hydrogen bond (N-O) distance and (N-H--O) angle for this interaction are 2.61 Å and 167°.

As revealed in Table 4, the ligand now has its greatest pair-wise interaction energy with Phe2.57(170) (−5.71 kcal/mol), followed by Lys3.28(192) (−4.94 kcal/mol), Leu7.43(387) (−4.14 kcal/mol), and Cys7.42(386) (−4.11 kcal/mol). The Phe2.57(170) interaction has significant van der Waals and coulombic contributions and seems to have arisen from the interaction of phenolic ring hydrogens with the aromatic ring of Phe2.57(170). The Lys3.28(192) interaction is dominated by the coulombic term, whereas the pair-wise interaction energies with Leu7.43(387) and Cys7.42(386) are dominated by the van der Waals term.

Table 4 also reveals that compared with its pair-wise energy of interaction in WT CB_1, HU210 has experienced a large decrease in pair-wise interaction energy upon the S7.39(383)A mutation. The ΔΔE is 10.03 kcal/mol [−38.10 kcal/mol − (−48.13 kcal/mol)]. As presented in Table 2, the binding affinity of HU210 in the S7.39(383)A mutant is diminished 102-fold. This significant decrease in ligand affinity may be due in part to this large decrease in pairwise interaction energy. It is important to note, however, that pairwise interaction energies may not be directly comparable with changes in affinities. The experimentally measured change in affinity includes not only the strength of ligand-receptor interactions in the newly formed complex but also the possible loss of intrareceptor interactions in the unoccupied receptor resulting from ligand binding. Although Table 4 should reflect the former, it does not take into consideration the latter.

CP55,940 at CB_1 S7.39(383)A R*. In the minimized WT CB_1 versus S7.39(383)A mutant bundles, the Cα to Cα TMH7 extracellular end distance is 2.64 Å. This measurement was taken using the Cα of Thr7.33(377), the last residue in TMH7. It is clear in Fig. 7 that in the energy-minimized HU210/S7.39(383)A CB_1 R* complex, the conformational shift in the extracellular portion of TMH7 (into the bundle) causes the extracellular ends of TMHs 1 and 2 to be displaced as well to accommodate this change in TMH7. Because CP55,940 lies higher in the TMH binding site crevice, the movement of the extracellular end of TMH7 into the bundle upon the S7.39(383)A mutation creates steric occlusion of the CP55,940 binding site. Docking studies indicate that this steric problem cannot be relieved by docking the second lowest energy minimum of CP55,940 or by rotating the A and C rings relative to one another about the C3-C1′ (Scheme 1) bond to some other torsion angle value.

Docking studies were also conducted to determine whether CP55,940 might be able to shift its position to that of HU210 in the S7.39(383)A mutant. In its global minimum energy conformation, however, CP55,940 has severe steric overlaps in the HU210 binding pocket. We then calculated the energy expense for CP55,940 to adopt an orientation of its A and C rings to mimic that of the A and C rings in HU210 (C1-C10b-

TABLE 4
Pairwise interaction energies for HU210 at CB_1 WT and S7.39(383)A mutant R* models

Residue	HU210/CB1 R*			HU210/CB1 S7.39A R*		
	VdW	Coulomb	Total	VdW	Coulomb	Total
	kcal/mol			*kcal/mol*		
Ser1.39	1.93	−7.14	−5.21	−0.09	−0.12	−0.20
Leu2.46	−0.58	−0.01	−0.59	−0.16	−0.02	−0.18
Asp2.50	−2.12	−0.69	−2.81	−1.45	−0.65	−2.10
Phe2.57	−2.46	−1.63	−4.09	−3.12	−2.59	−5.71
Ser2.60	−0.06	−0.02	−0.08	−0.28	−0.02	−0.30
Phe2.64	−0.91	−0.03	−0.94	−0.69	−0.09	−0.78
Lys3.28	0.70	−5.40	−4.70	3.05	−7.99	−4.94
Leu3.29	−0.79	0.06	−0.73	−0.68	0.06	−0.61
Val3.32	−2.32	−0.03	−2.35	−1.92	−0.03	−1.95
Ser3.35	−1.45	0.00	−1.45	−1.28	0.07	−1.22
Phe3.36	−1.90	0.08	−1.83	−1.70	0.09	−1.61
Ser3.39	−0.59	0.03	−0.56	−0.82	0.05	−0.77
Leu6.44	−0.09	0.00	−0.09	−0.48	0.02	−0.46
Cys6.47	−0.18	0.02	−0.17	−0.85	0.02	−0.83
Leu6.51	−0.85	−0.04	−0.89	−1.22	−0.02	−1.24
Ile6.54	−0.76	0.06	−0.69	−0.79	0.14	−0.64
Phe7.35	−0.18	0.01	−0.17	−0.28	0.00	−0.28
Ala7.36	−0.23	−0.13	−0.35	−0.19	−0.11	−0.29
Ser7.39	−0.45	−6.74	−7.19	−1.83	0.33	−1.51
Met7.40	−0.73	−0.19	−0.92	−0.86	0.09	−0.76
Cys7.42	−3.53	−0.71	−4.24	−3.53	−0.59	−4.11
Leu7.43	−4.07	−0.04	−4.11	−4.01	−0.13	−4.14
Asn7.45	−2.70	−0.26	−2.95	−2.35	−0.12	−2.47
Ser7.46	−0.64	−0.03	−0.66	−0.56	0.17	−0.39
Asn7.49	−0.59	0.06	−0.53	−0.58	0.07	−0.51
Water	−0.48	0.07	−0.41	−0.61	−0.04	−0.65
HU210 Conf Expense			0.59			0.59
Grand Total			−48.13			−38.10

C10a-C10 torsion angle = −56°). This expense was 4.43 kcal/mol at the Hartree Fock 3–21G* level. Steric clashes, however, still occurred for CP55,940 in this HU210-like conformation. These clashes were between C6 of the A ring and Ala7.39(383) and between the SAH group and Leu3.29(193) as well as Ile6.54(362). Thus, modeling studies indicate that the S7.39(383)A mutation prevents CP55,940 from docking in the CB_1 S7.39(383)A mutant model.

Discussion

In the present study, we have used computational modeling together with site-directed mutagenesis to explore the structural features of the hCB_1 receptor involved in determining the pharmacological activity of ligands of diverse chemical classes.

TABLE 5
Pairwise interaction energies for CP55,940 at CB_1 WT R* model

Res	VdW	Coulomb	Total
		kcal/mol	
Ile1.35	−0.47	−0.20	−0.66
Ala1.36	−0.59	−0.19	−0.78
Ser1.39	0.59	−6.26	−5.67
Asp2.50	−0.84	−0.21	−1.04
Gly2.53	−0.91	0.04	−0.87
Ile2.56	−1.15	0.09	−1.05
Phe2.57	−1.16	0.06	−1.10
Ser2.60	−1.07	0.64	−0.42
Phe2.64	−1.88	0.50	−1.38
Lys3.28	−0.41	−6.36	−6.77
Leu3.29	−0.42	0.00	−0.42
Gly3.31	−0.93	0.02	−0.91
Val3.32	−0.42	0.00	−0.43
Ser3.35	−0.41	0.04	−0.37
Lys(373)	−2.03	−12.88	−14.91
Ile(375)	−1.14	0.03	−1.11
Phe7.35	−1.12	0.16	−0.96
Ala7.36	−1.01	−0.44	−1.45
Ser7.39	−2.62	−1.55	−4.17
Met7.40	−1.44	−0.33	−1.76
Cys7.42	−0.39	0.14	−0.24
Leu7.43	−1.42	0.22	−1.20
Ser7.46	−0.21	0.02	−0.18
CP55,940			3.26
Grand total			−44.62

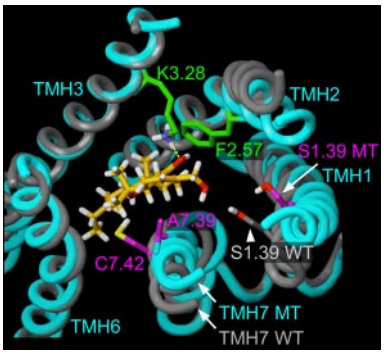

Fig. 7. The binding site of HU210 at the S7.39(383)A mutant. The S7.39(383)A mutant TMH bundle is shown in cyan. Residues with which the ligand has significant coulombic interactions are shown in green, whereas other selected residues in the binding pocket are shown in magenta. Yellow dashed lines indicate hydrogen bonding interactions. The WT CB_1 R* TMH bundle model (shown in gray) has been overlaid here to illustrate the shift in the positions of the extracellular portion of TMH7 and the resultant shift in the positions of the extracellular portions of TMHs 1 and 2 that occurs with the S7.39(383)A mutation. No significant shift was seen for any other TMH in the S7.39(383)A mutant relative to the WT TMH bundle. The position of S1.39 in WT CB_1 is also shown here in gray to illustrate the shift in S1.39 position that occurs upon the S7.39(383)A mutation. This shift precludes hydrogen bond formation with HU210 in the S7.39(383)A mutant.

The serine residues investigated here, Ser2.60 and Ser7.39 in the hCB_1 receptor, are also present at the equivalent position in the hCB_2 receptor (see Fig. 1A), suggesting that these residues may have a crucial structural and/or functional role. The S2.60A mutant receptor did not alter ligand affinity or receptor function, whereas the S7.39A mutant drastically altered the affinity and potency of CP55,940, HU210, and AM4056 but not that of the AAI, WIN55,212-2, and the inverse agonist SR141716A. Furthermore, neither mutant significantly altered the B_{max} value of the ligands tested (see Table 1). This suggests that no global alteration in receptor properties was induced as a consequence of the mutation.

In previous modeling studies of the isothiocyanate-labeled classic cannabinoid AM841, a ligand that covalently labels Cys6.47(357), we identified Ser7.39(383) and Ser2.60(173) as possible ligand interaction sites (Picone et al., 2005) for AM841. We were initially surprised to find that the S2.60A mutation did not affect receptor binding or function. We investigated the effect of (+)-7-OH-CBD-DMH, an active cannabidiol analog, at the S2.60A mutant, which has been postulated to form hydrogen-bonding interaction with Lys3.28 and Ser2.60A (R. Hart, D. Hurst, and P. Reggio, unpublished observations). The EC_{50} of (+)-7-OH-CBD-DMH-induced activation of the Ser2.60 mutant hCB_1 receptor in GTPγS functional assays was similar to WT hCB_1 (data not shown). Mutation studies reported here support Ser7.39(383), but not Ser2.60(173) as an important binding site residue for classic cannabinoids. These modeling studies indicate that when the C-3 alkyl tail of a classic cannabinoid is not tethered by covalent attachment, it can pull further into the TMH binding pocket. Whereas Ser7.39(383) still serves as a ligand interaction site, Ser1.39(123) is then preferred over Ser2.60(173) as an additional ligand interaction site.

In their sequence analyses of GPCRs, Mirzadegan et al. (2003) found that the frequency of occurrence of a serine at position 7.39 is only 4%. Our results here show that Ser7.39(383) in a $g-$ $\chi 1$ can induce a bend in TMH7 that moves the extracellular end of TMH7 away from the TMH bundle, creating a localized region where the structure of CB_1 and Rho (Palczewski et al., 2000) differ. This result is consistent with the proposal of Ballesteros et al. (2001) that although the overall structures of Rho and other class A GPCRs may be very similar, there may be localized regions where the structures of these receptors diverge.

The conformations of the TM7 helices chosen from our CM studies are consistent with the hypothesis that the presence of a Ser at position 7.39 in WT CB_1 TMH7 can induce a greater bend (15.1° in WT) compared with the S7.39(383)A mutant TMH7 (8.2°). This lessening of the bend angle facilitates the movement of the extracellular end of TMH7 in the S7.39(383)A mutant TMH7 into the bundle compared with WT and is probably the source of steric interference for CP55,940 in the S7.39(383)A mutant.

Our modeling results suggest that whereas CP55,940 and HU210 bind in the TMH1-2-3-7 region of the WT CB_1 binding pocket, CP55,940 binds higher (more extracellular) in this pocket (see Fig. 6c) and is therefore greatly affected by the inward movement of the extracellular end of TMH7 upon the S7.39(383)A mutation. At the CB_1 WT binding site identified

by modeling studies, CP55,940 is oriented with all three hydroxyls on the same face of the molecule. This orientation of the hydroxyls is consistent with the binding site model for CP55,940 proposed by Xie et al. (1996) based upon NMR solution spectra. Each of these hydroxyls finds a hydrogen bonding interaction in the CB_1 WT R* bundle model. The fact that one of these hydrogen bonds is with Lys3.28(192) is consistent with Lys3.28(192)A mutation data (Song and Bonner, 1996). In the docked position of CP55,940 illustrated in Fig. 6, c and d, the ring structure of CP55,940 is at and above (extracellular to) the level of Ser7.39(383). This docked position is consistent with mutation studies at Cys7.42(386) conducted in the Farrens' lab, which showed that enlargement of residue 7.42 (a residue that is intracellular to Ser7.39(383) and to the CP55,940 docking site) does not interfere with CP55,940 binding (Fay et al., 2005).

In addition to the profound effect the S7.39(383)A mutation has upon CP55,940 binding, the mutation also has a deleterious effect on the binding pocket of the classic cannabinoids, HU210 and AM4056 (results not shown), causing the loss of two hydrogen bonds for HU210 (see Fig. 7). However, the binding of WIN55,212-2 and SR141716A are unchanged by this mutation. Our combined mutation and modeling studies have shown that the binding pocket for WIN55,212-2 is within the CB_1 aromatic microdomain formed by TMH3-4-5–6 (McAllister et al., 2003). Given that the WIN55,212-2 binding pocket is removed from the TMH1-2-7 region, the S7.39(383)A mutation and its resultant conformational effect on the extracellular end of TMH7 (and indirectly on TMHs 1 and 2) would not therefore be expected to affect WIN55,212-2 binding.

Our studies of the binding pocket for the CB_1 inverse agonist SR141716A have indicated that although the aromatic portions of this ligand bind in the TMH3-4-5-6 aromatic microdomain, the piperidine ring of SR141716A lies between TMH3 and TMH7 directly beneath Ser7.39(383) and above Cys7.42(386) (Hurst et al., 2002, 2006; McAllister et al., 2003). This docked position is consistent with mutation studies at Cys7.42(386) conducted in the Farrens' lab showing that enlargement of residue 7.42 interferes with SR141716A binding (Fay et al., 2005). However, SR141716A would not be affected by the change induced by the S7.39(383)A mutation, because the piperidine resides below (i.e., intracellular to) residue 7.39. Thus, consistent with results reported here, any changes induced by mutation of Ser7.39(383) would not be expected to affect SR141716A binding.

In the CB_2 receptor, mutation of the homologous Ser285 (Ser7.39) residue has been reported to decrease the binding affinity of the classic agonist HU-243 (Rhee, 2002). However, the ability of HU210, CP55,940, and WIN55,212-2 to inhibit adenyl cyclase was similar to that of wild type. In contrast, the author reports Ser292 (Ser7.46) to be involved in the binding of HU210 and CP55,940 and not WIN5512–2 via a hydrogen-bonding interaction. Furthermore, Rhee (2002) measured IC_{50} value as a measure of the binding affinity, a value that intrinsically depends on the agonist concentration that is employed. The use of inhibitory constant (K_i) value (see *Materials and Methods*) instead should give a better estimate of ligand affinity. Moreover, our observations with Ser7.39 (homologous to Ser285 in CB_2 receptor) were in the hCB_1 receptor; it is difficult, therefore, to correlate the two sets of results.

The Ser7.39 mutant receptor resulted in a profound shift in agonist sensitivity (50- to 100-fold) and potency (200- to 500-fold) toward a higher concentration that was selective for HU210 and AM4056. The S7.39A mutant resulted in no detectable CP55,940 binding in saturation binding assays using [^{3}H]CP55,940 as the reporter radioligand (see Table 1). However, in competition studies on the S7.39A mutant, some displacement by CP55,940 was observed at high concentrations. However, this observation seems counter-intuitive given the fact that in saturation binding studies, no detectable CP55,940 binding was observed. It should be noted that this partial displacement (~40%) observed is prone to errors as a result of the limitations of high concentrations (10 μM) of CP55,940 used. Likewise, serine-to-alanine mutations in the β_2-adrenergic receptor have been demonstrated to shift the equilibrium from active to inactive receptor state by attenuating the constitutive activity of the receptor (Ambrosio et al., 2000). Our modeling results clearly demonstrate that the S7.39A mutation removes or reduces the kink of the α-helix, thereby causing a local perturbation of structure in the TMH6-EC3-TMH7 region. This mutation consequently affects ligands that incorporate the above region as part of their binding pocket, such as CP55,940, HU210, and AM4056 but not WIN55,212-2 and SR141716A.

Although caveats must be placed on interpreting conclusions from mutagenesis experiments because the mutation created may have affected ligand binding or the subsequent coupling of ligand binding to signal transduction mechanisms, our in silico modeling studies validate the in vitro mutagenesis results. In summary, we have identified a residue, Ser7.39, the mutation of which (to S7.39A) results in a total ablation of CP55,940 binding and significant decrease in the affinity and potency for HU210 and AM4056. This residue from TMH 7 has not previously been implicated in modulating the hCB_1 receptor function. In the absence of a crystal structure of the CB_1 receptor, combining the receptors' structural information with functional experiments will assist in the identification of residues involved in ligand binding and provide valuable mechanistic insights in the functioning of the receptor. In addition, these receptor structure-function studies can help in the development of ligands with high specificity for the receptor.

References

Abood ME (2005) Molecular biology of cannabinoid receptors. *Handb Exp Pharmacol* **(168):**81–115.

Ambrosio C, Molinari P, Cotecchia S, and Costa T (2000) Catechol-binding serines of β_2-adrenergic receptors control the equilibrium between active and inactive receptor states. *Mol Pharmacol* **57:**198–210.

Arnis S, Fahmy K, Hofmann KP, and Sakmar TP (1994) A conserved carboxylic acid group mediates light-dependent proton uptake and signaling by rhodopsin. *J Biol Chem* **269:**23879–23881.

Ballesteros JA, Deupi X, Olivella M, Haaksma EE, and Pardo L (2000) Serine and threonine residues bend alpha-helices in the chi(1) = $g(-)$ conformation. *Biophys J* **79:**2754–2760.

Ballesteros JA, Shi L, and Javitch JA (2001) Structural mimicry in G protein-coupled receptors: implications of the high-resolution structure of rhodopsin for structure-function analysis of rhodopsin-like receptors [published erratum appears in *Mol Pharmacol* **61:**247, 2002]. *Mol Pharmacol* **60:**1–19.

Ballesteros JA and Weinstein H (1995) Integrated methods for the construction of three dimensional models and computational probing of structure function relations in G protein-coupled receptors, in *Methods in Neuroscience* (Conn PM and Sealfon SM eds) pp 366–428, Academic Press, San Diego.

Barnett-Norris J, Hurst DP, Buehner K, Ballesteros JA, Guarnieri F, and Reggio PH (2002) Agonist alkyl tail interaction with cannabinoid CB1 receptor V6.43/I6.46 groove induces a Helix 6 active conformation. *Int J Quantum Chem* **88:**76–86.

Barnett-Norris J, Hurst DP and Reggio PH (2003) The influence of cannabinoid receptor second extracellular loop conformation on the binding of CP55940, in *2003 Symposium on the Cannabinoids*, p 79, International Cannabinoid Research Society, Cornwall, Ontario.

Bramblett RD, Panu AM, Ballesteros JA, and Reggio PH (1995) Construction of a 3D

model of the cannabinoid CB1 receptor: determination of helix ends and helix orientation. *Life Sci* **56:**1971–1982.
Cheng Y and Prusoff WH (1973) Relationship between the inhibition constant (K1) and the concentration of inhibitor which causes 50 per cent inhibition (I50) of an enzymatic reaction. *Biochem Pharmacol* **22:**3099–3108.
Chin C, Abadji V, Lucas-Lenard J, and Kendall D (1998) Ligand binding and modulation of cyclic AMP levels depends on the chemical nature of residue 192 of the human cannabinoid receptor 1. *J Neurochem* **70:**366–373.
D'Antona AM, Ahn KH, and Kendall DA (2006) Mutations of CB(1) T210 produce active and inactive receptor forms: correlations with ligand affinity, receptor stability, and cellular localization. *Biochemistry* **45:**5606–5617.
Farrens D, Altenbach C, Ynag K, Hubbell W, and Khorana H (1996) Requirement of rigid-body motion of transmembrane helices for light activation of rhodopsin. *Science (Wash DC)* **274:**768–770.
Fay JF, Dunham TD, and Farrens DL (2005) Cysteine residues in the human cannabinoid receptor: only C257 and C264 are required for a functional receptor, and steric bulk at C386 impairs antagonist SR141716A binding. *Biochemistry* **44:**8757–8769.
Felder CC, Joyce KE, Briley EM, Mansouri J, Mackie K, Blond O, Lai Y, Ma AL, and Mitchell RL (1995) Comparison of the pharmacology and signal transduction of the human cannabinoid CB1 and CB2 receptors. *Mol Pharmacol* **48:**443–450.
Fiser A, Do RK, and Sali A (2000) Modeling of loops in protein structures. *Protein Sci* **9:**1753–1773.
Gérard CM, Mollereau C, Vassart G, and Parmentier M (1991) Molecular cloning of a human cannabinoid receptor which is also expressed in testis. *Biochem J* **279:** 129–134.
Ghanouni P, Steenhuis JJ, Farrens DL, and Kobilka BK (2001) Agonist-induced conformational changes in the G-protein-coupling domain of the beta 2 adrenergic receptor. *Proc Natl Acad Sci USA* **98:**5997–6002
Gouldson PR, Kidley NJ, Bywater RP, Psaroudakis G, Brooks HD, Diaz C, Shire D, and Reynolds CA (2004) Toward the active conformations of rhodopsin and the beta2-adrenergic receptor. *Proteins* **56:**67–84.
Gratkowski H, Lear JD, and DeGrado WF (2001) Polar side chains drive the association of model transmembrane peptides. *Proc Natl Acad Sci USA* **98:**880–885.
Gray TM and Matthews BW (1984) Intrahelical hydrogen bonding of serine, threonine and cysteine residues within alpha helices and its relevance to membrane-bound proteins. *J Mol Biol* **175:**75–81.
Guarnieri F and Weinstein H (1996) Conformational memories and the exploration of biologically relevant peptide conformations: an illustration for the gonadotropin-releasing hormone. *J Am Chem Soc* **118:**5580–5589.
Hassan SA, Guarnieri F, and Mehler EL (2000a) Characterization of hydrogen bonding in a continuum solvent model. *J Phys Chem B* **104:**6490–6498.
Hassan SA, Guarnieri F, and Mehler EL (2000b) A general treatment of solvent effects based on screened coulomb potentials. *J Phys Chem B* **104:**6478–6489.
Hassan SA, Mehler EL, and Weinstein H (2002) Structure calculation of protein segments connecting domains with defined secondary structure: A simulated annealing Monte Carlo combined with biased scaled collective variables technique, in *Computational Methods for Macromolecules: Challenges and Applications* (Gan HH ed) pp 197–231, Springer Verlag, New York.
Howlett AC, Barth F, Bonner TI, Cabral G, Casellas P, Devane WA, Felder CC, Herkenham M, Mackie K, Martin BR, et al. (2002) International Union of Pharmacology. XXVII. Classification of cannabinoid receptors. *Pharmacol Rev* **54:**161–202.
Huffman JW, Yu S, Showalter V, Abood ME, Wiley JL, Compton DR, Martin BR, Bramblett RD, and Reggio PH (1996) Synthesis and Pharmacology of a very potent cannabinoid lacking a phenolic hydroxyl with high affinity for the CB2 receptor. *J Med Chem* **39:**3875–3877.
Hurst D, Umejiego U, Lynch D, Seltzman H, Hyatt S, Roche M, McAllister S, Fleischer D, Kapur A, Abood M, et al. (2006) Biarylpyrazole inverse agonists at the cannabinoid CB1 receptor: importance of the C-3 carboxamide oxygen/lysine3.28(192) interaction. *J Med Chem* **49:**5969–5987.
Hurst DP, Lynch DL, Barnett-Norris J, Hyatt SM, Seltzman HH, Zhong M, Song ZH, Nie J, Lewis D, and Reggio PH (2002) *N*-(Piperidin-1-yl)-5-(4-chlorophenyl)-1-(2,4-dichlorophenyl)-4-methyl-1*H*-pyrazole-3-carboxamide (SR141716A) Interaction with LYS 3.28(192) Is crucial for its inverse agonism at the cannabinoid CB1 receptor. *Mol Pharmacol* **62:**1274–1287.
Javitch JA, Fu D, Liapakis G, and Chen J (1997) Constitutive activation of the b2 adrenergic receptor alters the orientation of its sixth membrane-spanning segment. *J Biol Chem* **272:**18546–18549.
Jensen AD, Guarnieri F, Rasmussen SG, Asmar F, Ballesteros JA, and Gether U (2001) Agonist-induced conformational changes at the cytoplasmic side of transmembrane segment 6 in the β2 adrenergic receptor mapped by site-selective fluorescent labeling. *J Biol Chem* **276:**9279–9290.
Li J, Edwards PC, Burghammer M, Villa C, and Schertler GF (2004) Structure of bovine rhodopsin in a trigonal crystal form. *J Mol Biol* **343:**1409–1438.
Lin SW and Sakmar TP (1996) Specific tryptophan UV-absorbance changes are probes of the transition of rhodopsin to its active state. *Biochemistry* **35:**11149–11159.
McAllister SD, Hurst DP, Barnett-Norris J, Lynch D, Reggio PH, and Abood ME (2004) Structural mimicry in class A G protein-coupled receptor rotamer toggle switches: the importance of the F3.36(201)/W6.48(357) interaction in cannabinoid CB1 receptor activation. *J Biol Chem* **279:**48024–48037.
McAllister SD, Rizvi G, Anavi-Goffer S, Hurst DP, Barnett-Norris J, Lynch DL, Reggio PH, and Abood ME (2003) An aromatic microdomain at the cannabinoid CB(1) receptor constitutes an agonist/inverse agonist binding region. *J Med Chem* **46:**5139–5152.
McAllister SD, Tao Q, Barnett-Norris J, Buehner K, Hurst DP, Guarnieri F, Reggio PH, Nowell Harmon KW, Cabral GA, and Abood ME (2002) A critical role for a tyrosine residue in the cannabinoid receptors for ligand recognition. *Biochem Pharmacol* **63:**2121–2136.
Melvin LS, Milne GM, Johnson MR, Subramaniam B, Wilken GH, and Howlett AC (1993) Structure-activity relationships for cannabinoid receptor-binding and analgesic activity: studies of bicyclic cannabinoid analogs. *Mol Pharmacol* **44:**1008–1015.
Mirzadegan T, Benko G, Filipek S, and Palczewski K (2003) Sequence analyses of G-protein-coupled receptors: similarities to rhodopsin. *Biochemistry* **42:**2759–2767.
Mohamadi F, Richards N, Guida W, Liskamp R, Lipton M, Caulfield C, Chang G, Hendrickson T, and Still W (1990) MacroModel- an integrated software system for modeling organic and bioorganic molecules using molecular mechanics. *J Comput Chem* **11:**440–467.
Munro S, Thomas KL, and Abu-Shaar M (1993) Molecular characterization of a peripheral receptor for cannabinoids. *Nature (Lond)* **365:**61–65.
Nakanishi J, Takarada T, Yunoki S, Kikuchi Y, and Maeda M (2006) FRET-based monitoring of conformational change of the beta2 adrenergic receptor in living cells. *Biochem Biophys Res Commun* **343:**1191–1196.
Okada T, Fujiyoshi Y, Silow M, Navarro J, Landau EM, and Shichida Y (2002) Functional role of internal water molecules in rhodopsin revealed by X-ray crystallography. *Proc Natl Acad Sci USA* **99:**5982–5987.
Palczewski K, Kumasaka T, Hori T, Behnke CA, Motoshima H, Fox BA, Le Trong I, Teller DC, Okada T, Stenkamp RE, et al. (2000) Crystal structure of rhodopsin: A G protein-coupled receptor. *Science (Wash DC)* **289:**739–745.
Picone RP, Fournier DJ, and Makriyannis A (2002) Ligand based structural studies of the CB1 cannabinoid receptor. *J Pept Res* **60:**348–356.
Picone RP, Khanolkar AD, Xu W, Ayotte LA, Thakur GA, Hurst DP, Abood ME, Reggio PH, Fournier DJ, and Makriyannis A (2005) (−)-7′-Isothiocyanato-11-hydroxy-1′,1′-dimethylheptylhexahydrocannabinol (AM841), a high-affinity electrophilic ligand, interacts covalently with a cysteine in helix six and activates the CB1 cannabinoid receptor. *Mol Pharmacol* **68:**1623–1635.
Price MR, Baillie GL, Thomas A, Stevenson LA, Easson M, Goodwin R, McLean A, McIntosh L, Goodwin G, Walker G, et al. (2005) Allosteric modulation of the cannabinoid CB1 receptor. *Mol Pharmacol* **68:**1484–1495.
Reggio PH (2005) Cannabinoid receptors and their ligands: ligand-ligand and ligand-receptor modeling approaches. *Handb Exp Pharmacol* **(168):**247–281.
Reggio PH, Panu AM, and Miles S (1993) Characterization of a region of steric interference at the cannabinoid receptor using the active analog approach. *J Med Chem* **36:**1761–1771.
Rhee MH (2002) Functional role of serine residues of transmembrane dopamin VII in signal transduction of CB2 cannabinoid receptor. *J Vet Sci* **3:**185–191.
Sali A and Blundell TL (1993) Comparative protein modelling by satisfaction of spatial restraints. *J Mol Biol* **234:**779–815.
Salo OM, Lahtela-Kakkonen M, Gynther J, Jarvinen T, and Poso A (2004) Development of a 3D model for the human cannabinoid CB1 receptor. *J Med Chem* **47:**3048–3057.
Salom D, Lodowski DT, Stenkamp RE, Trong IL, Golczak M, Jastrzebska B, Harris T, Ballesteros JA, and Palczewski K (2006) Crystal structure of a photoactivated deprotonated intermediate of rhodopsin. *Proc Natl Acad Sci USA* **103:**16123–16128.
Schertler GF (2005) Structure of rhodopsin and the metarhodopsin I photointermediate. *Curr Opin Struct Biol* **15:**408–415.
Shi L, Liapakis G, Xu R, Guarnieri F, Ballesteros JA, and Javitch JA (2002) Beta 2 adrenergic receptor activation. Modulation of the proline kink in transmembrane 6 by a rotamer toggle switch. *J Biol Chem* **277:**40989–40996.
Song Z-H and Bonner TI (1996) A lysine residue of the cannabinoid receptor is critical for receptor recognition by several agonists but not WIN55212–2. *Mol Pharmacol* **49:**891–896.
Szundi I, Ruprecht JJ, Epps J, Villa C, Swartz TE, Lewis JW, Schertler GF, and Kliger DS (2006) Rhodopsin photointermediates in two-dimensional crystals at physiological temperatures. *Biochemistry* **45:**4974–4982
Tao Q, McAllister S, Andreassi J, Nowell K, Cabral G, Hurst D, Bachtel K, Ekman M, Reggio P, and Abood M (1999) Role of a conserved lysine residue in the peripheral cannabinoid receptor (CB2): evidence for subtype specificity. *Mol Pharmacol* **55:**605–613.
Ulfers AL, McMurry JL, Kendall DA, and Mierke DF (2002) Structure of the third intracellular loop of the human cannabinoid 1 receptor. *Biochemistry* **41:**11344–11350.
Visiers I, Braunheim BB, and Weinstein H (2000) Prokink: a protocol for numerical evaluation of helix distortions by proline. *Protein Eng* **13:**603–606.
Ward SD, Hamdan FF, Bloodworth LM, Siddiqui NA, Li JH, and Wess J (2006) Use of an in situ disulfide cross-linking strategy to study the dynamic properties of the cytoplasmic end of transmembrane domain VI of the M(3) muscarinic acetylcholine receptor. *Biochemistry* **45:**676–685.
Xie XQ, Melvin LS, and Makriyannis A (1996) The conformational properties of the highly selective cannabinoid receptor ligand CP-55,940. *J Biol Chem* **271:**10640–10647.
Zhang R, Hurst DP, Barnett-Norris J, Reggio PH, and Song ZH (2005) Cysteine 2.59(89) in the second transmembrane domain of human cb2 receptor is accessible within the ligand binding crevice: evidence for possible CB2 deviation from a rhodopsin template. *Mol Pharmacol* **68:**69–83.

Address correspondence to: Dr. Mary E. Abood, California Pacific Medical Center Research Institute, San Francisco, CA 94107. E-mail: aboodm@cpmcri.org